

Characteristics of Transmission Radio Waves in Undulating Coal Seams and a Topographic Correction Method For Its Tomography

Rongxin WU

Anhui University of Science and Technology

Huanqi GU

Anhui University of Science and Technology

zean hu (✉ zahu@aust.edu.cn)

Anhui University of Science and Technology

Case study

Keywords: Undulating coal seam, radio wave penetration, tomography, undulating correction

Posted Date: June 30th, 2021

DOI: <https://doi.org/10.21203/rs.3.rs-659049/v1>

License:   This work is licensed under a Creative Commons Attribution 4.0 International License.

[Read Full License](#)

1 Characteristics of transmission radio waves in undulating coal seams and a topographic
2 correction method for its tomography

3
4 Rongxin Wu ^{1,2}, Huanqi Gu ¹, Zean Hu ¹

5
6 ¹ School of Earth and Environment, Anhui University of Science and Technology, Huainan, Anhui,
7 232001

8 ² State Key Laboratory of Mining Response and Disaster Prevention and Control in Deep Coal
9 Mines, Huainan, Anhui, 232001

10
11 **Abstract**

12 The transparency of coal seam working face is an important assurance for safe and accurate
13 mining of coal mines. Mine geophysical prospecting is an important means for geological
14 exploration of coal seam working faces, among which the mine radio wave tomography is one of
15 the most common and effective methods. However, the undulating feature of the coal seam will
16 greatly interfere the high-precision attenuation electromagnetic wave imaging. Through two-
17 dimensional numerical simulation experiments, we identified that in a horizontal coal seam, the
18 energy of penetrated radio wave showed an approximate linear attenuation law, while in an
19 inclined coal seam, it showed a very different parabolic attenuation trend. To eliminate the
20 influence of coal seam inclination on the accuracy of radio wave tomography, in this paper, we
21 proposed a correction method for imaging undulating coal seams using radio wave tomography.
22 Further, through three-dimensional numerical simulation experiments, we verified the validity and
23 reliability of the correction method. Overall, both theoretical and numerical simulation
24 experiments indicated that the method could basically eliminate the influence of coal seam
25 inclination and improve the imaging accuracy.

26
27 **Keywords:** Undulating coal seam; radio wave penetration; tomography; undulating correction

28

29

30

31

32

33 **Introduction**

34 Coal is the main energy source of China and provides important support for the sustainable
35 development of China's economy. Although the energy structure is constantly changing with the
36 development of the social economy, coal consumption still accounts for 80% of China's total
37 energy consumption. Therefore, coal's dominant position in the energy structure will not change
38 in a short period of time (Peng et al., 2015). Nowadays, with the popularization of industrialization,
39 the realization of precise and intelligent coal mining has become the only way for mining. This
40 means that identification of geological anomalies in the working face and the transparency of the
41 geological conditions of the mine working face are important foundations for intelligent and
42 precise coal mining (Yuan et al., 2019; Cheng et al., 2019). The current methods used to explore
43 the geological structures of the working face include the cross-well electromagnetic method,
44 channel wave exploration, and seismic tomography. However, the current ordinary drilling and
45 geophysical exploration methods can no longer meet the requirements for high-precision
46 exploration and are unable to accurately detect some hidden structures as well as faults with a drop
47 of less than 5 m (Hu et al., 2017). Accurate detection of geological structures in coal seam working
48 faces urgently requires high-precision detection methods to improve the economic benefits and
49 mining safety of the coal mine.

50 Radio wave tomography is one of the most effective and universal methods for detecting the
51 geological structures of coal seam working face. Many scholars have theoretically explored the
52 radio wave propagation laws and imaging algorithms. In terms of propagation laws, researchers
53 proposed the layered geoelectric model and the single medium model, where the electrical changes
54 of the top and bottom of the coal seam and the thickness of the coal seam will affect the phase of
55 radio wave (Stolarczyk et al., 2003; Hussain et al., 2011). For complex coal mining faces, the ray

56 tracing-based radio waves propagation (RTRWP) law can effectively describe the radio wave
57 propagation environment (Zhao et al., 2013). In terms of imaging algorithms, an improved Land
58 Weber method was derived by improving the condition number of the weighting matrix and
59 introducing new L1 norm and the objective function of the regularization term, which has better
60 performance in typical modes and improves the space resolution (Han et al., 2018; Liu et al. 2019).

61 Among them, imaging with improved attenuation coefficient P can improve the detection accuracy
62 in practical application (Liu et al., 2013), and phase tomography is considered as a rapid, effective
63 new electromagnetic wave inversion method (Liu et al., 2013; Yu et al., 2011). In addition,
64 determination of the initial field strength is also a useful attempt to improve the accuracy of radio
65 wave tomography (Zhang et al., 2016), and the effective penetration width of the working surface
66 can be determined from the initial field strength, absorption coefficient and background field
67 strength (Xiao et al., 2017). Decades of research and application have proven that the
68 electromagnetic wave method can effectively detect faults, collapsed columns, coal seam thinning
69 areas, karst development, broken zones, and other geological hazards in coal seams (Hatherly et
70 al., 2013; Li et al., 2015).

71 Radio wave tomography is advantageous in simple operation and good detection success.
72 However, there are still issues such as incomplete understanding of radio waves propagation law
73 in coal seams, simplicity of the collected electromagnetic parameters, and low imaging accuracy
74 (Xiao et al. 2017; Zhang et al., 2017). The cause for the low accuracy of radio wave tomography
75 is partly the influence of coal seam undulations. At present, in the studies on the geological
76 structure of underground coal seam working face with different computed tomography techniques,
77 the undulation degree of coal seam between roadways is rarely considered, making a great
78 difference in the actual results (Hu et al., 2019). Fully analyzing the propagation characteristics
79 and influencing factors of the radio waves in undulating coal seams is an effective way to improve
80 the cognition and exploration accuracy of radio wave field in coal seams. Due to the inclination,
81 there is a certain elevation difference between the radio wave transmitters and the receivers. Thus,
82 it is necessary to propose a tomographic imaging method that can eliminate the influence of
83 elevation difference to eliminate the influence of coal seam undulation on radio wave imaging data
84 processing and interpretation. In this study, based on ray tracing, we proposed a quasi-three-

85 dimensional (3D) tomographic imaging technology to solve the deviation issue of imaging results
 86 caused by coal seam undulations to improve the accuracy of radio wave tomography.

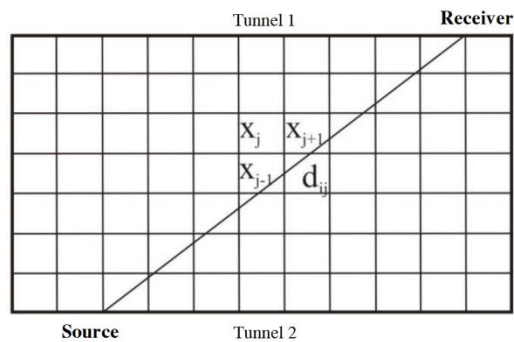
87

88 **1 Introduction to the principle of radio wave tomography**

89

90 Radio wave tomography is a detection method by emitting radiofrequency electromagnetic
 91 waves. It has also been named as radio wave penetration method and electromagnetic wave
 92 tomography (Liu et al. 2020). Fullagar et al. collectively refer to it as the radio imaging method or
 93 RIM for short (Fullagar et al., 2000). Its main theoretical basis is energy attenuation tomography
 94 based on ray tracing, which uses sinusoidal electromagnetic waves as the emission source to obtain
 95 the distribution of the absorption coefficient of the medium. At present, the commonly used
 96 frequencies of mainstream electromagnetic wave penetration instruments are 88 kHz, 158 kHz,
 97 365 kHz, and 965 kHz (Xiao et al., 2017). The essence of the radio wave penetration imaging of
 98 the working face is to solve an ill-conditioned linear equation system (Liu et al., 2017). The
 99 intensity H of the electromagnetic wave in the coal seam at any point is expressed as:

100
$$H_m = H_0 \frac{e^{-\beta r}}{r} \sin \theta \quad (1)$$



101

102 Fig.1 Schematic diagram of tomography grid (Liu et al., 2013)

103

104 The imaging space in the working surface is gridded. In this area, a ray y_i passes through the
 105 pixels with the field strength attenuation coefficients being x_1, x_2, \dots, x_n , and the intercepts on these

106 pixels being $d_{i1}, d_{i2}, \dots, d_{in}$. In this way, the electromagnetic wave energy attenuation value \mathbf{VH}_i on
 107 the i -th ray path can be expressed as:

$$108 \quad \mathbf{VH}_i = \sum_{j=1}^n d_{ij} x_j \quad (2)$$

109 The energy attenuation value \mathbf{VH}_i can be obtained from the measured value and the correction
 110 value $8.68 \ln r_i$ (Xiao et al. 2017):

$$111 \quad \sum_{j=1}^n d_{ij} x_j = H_0 - 8.68 \ln r_i - H_i \quad (3)$$

112 In the coal seam working face, the radio wave is emitted from multiple points, and the coal
 113 mining face is covered multiple times. By performing multi-point receiving measurement on each
 114 source, one can get the matrix equation of the following large sparse matrix:

$$115 \quad \begin{bmatrix} d_{11} & d_{12} & L & d_{1n} \\ d_{21} & d_{22} & L & d_{2n} \\ M & M & L & M \\ d_{n1} & d_{n2} & L & d_{nn} \end{bmatrix} \begin{bmatrix} x_1 \\ x_2 \\ M \\ x_n \end{bmatrix} = \begin{bmatrix} \mathbf{VH}_1 \\ \mathbf{VH}_2 \\ M \\ \mathbf{VH}_n \end{bmatrix} \quad (4)$$

117
 118 **2. Principle of radio wave tomography correction method for undulating coal seams**

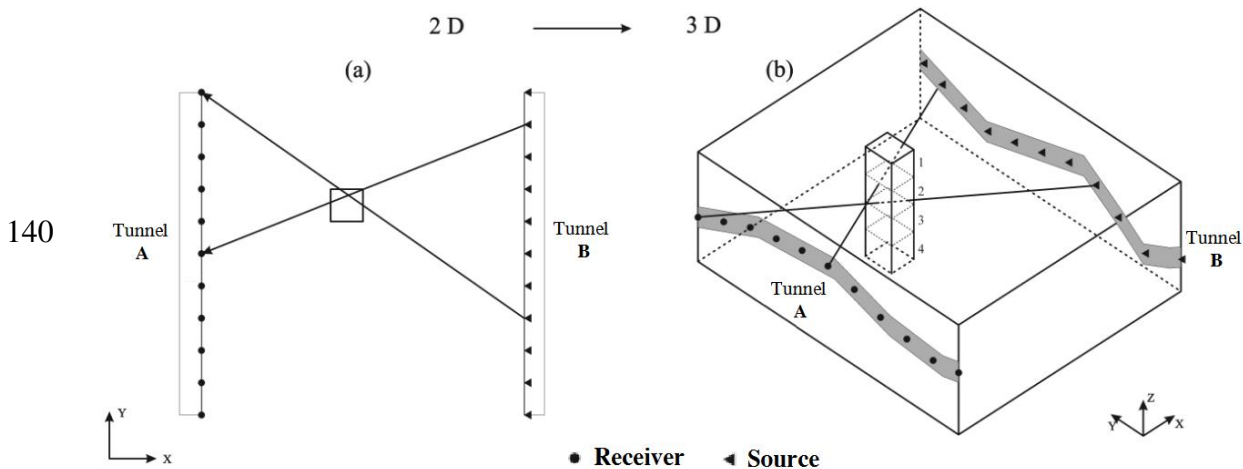
119 2.1 The impact of coal seam undulation

120 3D penetration tomography is a more feasible method to overcome the influence of coal seam
 121 inclination on radio wave tomography. But this method still has some unsolved difficulties in the
 122 inversion of the radio wave computed tomography in coal mines. Jackson et al. used boreholes on
 123 the ground construction to perform cross-hole velocity tomography for inversion to obtain the 3D
 124 structural characteristics of coal seams (Jackson et al. 1995). Due to the limited numbers of
 125 boreholes, the data density in the horizontal direction is not enough, which in turn causes the
 126 underdetermined problem of the velocity equation. The same problem also presents in the 3D radio
 127 wave tomography between two roadways. Since the signal source and receiver are both arranged

128 in the roadway, the data in the depth direction is not enough. Therefore, the underdetermined
129 problem of the absorption coefficient equation is more serious.

130 When performing radio wave penetration tomography of coal seam working surface, the data
131 volume of radio wave penetration field strength is often insufficient due to the limitation of the
132 test space. When performing 2D imaging inversion, because the coal seam undulation is not
133 considered, the number of grids required for inversion is small, and the amount of data is just
134 enough, as shown in Fig.2-1a. Therefore, when switching from 2D inversion to 3D inversion,
135 multiple grids must be set in the Z direction, as shown in Fig.2-1b. Due to the lack of data, the rays
136 can only pass through a part of the grids. For example, in Fig.2-1b, only grids 1 and 2 have data
137 lines passing through, while grids 3 and 4 do not. This phenomenon will greatly aggravate the
138 under-determinism of the matrix equation.

139



141

142 Fig.2 Schematic diagram of the underdetermined equation of 3D tomography of coal seam
143 working face

144

145 2.2 The method to solve the influence of coal seam undulation

146 3D penetration tomography requires sufficient data in the vertical direction. But the
147 measurement conditions of the coal seam working face are unable to meet the requirement. Based

148 on the current technical conditions, we proposed a technical scheme similar to the 3D attenuation
149 coefficient electromagnetic penetration tomography. The essence of this scheme is a simplified 3D
150 inversion model, that is, a plate-shaped inversion model with only one large grid in the vertical
151 direction. The solution adds an elevation parameter to make the ray tracing travel path more
152 accurate. Meanwhile, the number of grids in the Z axis direction is 1, making the electrical model
153 essentially 2D, thereby solving the problem of an underdetermined 3D attenuation coefficient
154 equation.

155 2.2.1 Ray tracing

156 Ray tracing is a common forward modeling method with very concise and intuitive
157 calculation. It is often used to indicate the ray propagation path in complex geological conditions.
158 These methods are mostly based on the least attenuation between 3D adjacent grid nodes. For
159 example, the 3D finite difference ray tracing method calculates and selects the minimum
160 attenuation between seven adjacent grid nodes. Because the pseudo-3D model has only one grid in
161 the Z direction, the 3D finite difference ray tracing is obviously not applicable. To this end, we first
162 performed a 2D ray tracing on the XY plane of the model and brought in the even elevation
163 difference between the source points and the receiving points to calculate the ray length in each 3D
164 grid. The finite difference method first requires the numerical model to be meshed discretely. The
165 equation is then constructed through the dB value of the known grid nodes. Solving the equation
166 can obtain the dB value of other nodes in the grid. So, the dB value of adjacent nodes is obtained
167 according to the above method, and the dB value of all grid nodes in the model is calculated by
168 repeating the above process. According to the smallest change direction of the dB value, that is,
169 the smallest attenuation coefficient, the propagation path of radio wave penetration in the model
170 can be obtained. Further, according to the known relative position relationship between the source
171 and the receiver, the length d_{ij} of the i-th ray in the j-th grid can be obtained in 2D condition.
172 Knowing the elevation difference h_i of the i-th ray, by adding the average of the total elevation
173 difference to the passing M grids, one can get the ray length D_{ij} in 3D condition.

174

175

$$D_{ij} = \sqrt{d_{ij}^2 + \left(\frac{h_i}{M}\right)^2} \quad (5)$$

176

177 2.2.2 Construction of the inversion equation and related calculation

178 Based on the above ray tracing results, the expression of radio wave energy attenuation is

$$179 \quad \forall H_i = \sum_{j=1}^M D_{ij} x_j \quad (i = 1, \dots, N) \quad (6)$$

180 where x_j is the electromagnetic wave energy attenuation coefficient in the j -th grid, D_{ij} is the length
181 of the j -th grid on the i -th ray, N is the total number of rays, and M is the number of grids.

182 At this time, a grid matrix $A(N \times M)$ can be established in the detection area, forming the
183 following matrix equation:

$$184 \quad x = A^{-1} \forall H \quad (7)$$

185 Solving the coefficient matrix of Eq.7 can obtain the distribution information of the attenuation
186 coefficient in the detection area. Many methods have been proposed to obtain the coefficient
187 matrix. Of them, the most commonly used methods include the algebraic reconstruction technique
188 (ART), simultaneous iterative reconstruction technique (SIRT), least square QR decomposition
189 (LSQR), and singular value decomposition (SVD). Because SIRT has advantages such as better
190 convergence speed, good calculation efficiency, and solution stability, it is adopted in the inversion
191 calculation in this study.

192 3. 2D numerical simulation experiments

193 3.1 Theoretical basis of GprMax forward simulation

194 GprMax software was used to carry out the numerical simulation calculation of the radio
195 wave tomography. GprMax software is a 2D and 3D numerical simulation software for
196 electromagnetic waves based on finite difference time domain (FDTD) algorithm and perfectly
197 matching layer (PML) absorbing boundary conditions (Giannopoulos 1997; Yee 1966). The
198 software can simulate the field distribution of electromagnetic waves in different relative
199 permittivity media and anomalous body models to obtain electromagnetic wave response signals
200 of underground layers and anomalies.

201 3.2 Forward simulation of the horizontal coal seams

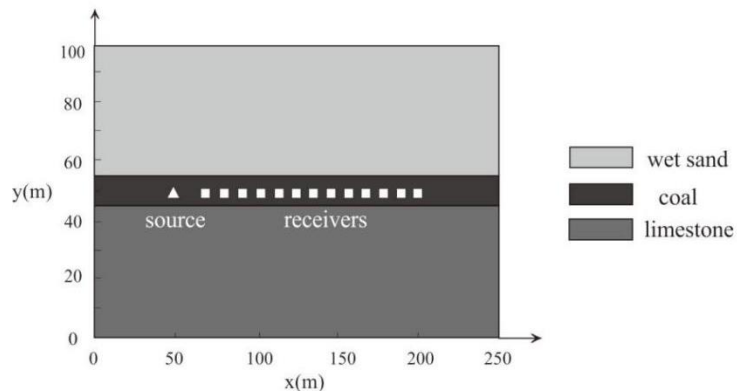
202 To fully understand the propagation law and wave field characteristics of radio waves in coal
 203 seams, it is necessary to construct a 2D electrical property model of coal-measure formation and
 204 analyze the factors affecting radio wave propagation through electromagnetic wave simulation
 205 data. Table 1 shows the lithology of the coal seam as well as its roof and floor and the typical
 206 electrical parameters of non-magnetic conventional media (Jol 2011).

207 Table 1 Parameters of media used in the model

Items	Relative permittivity ϵ_r	Relative conductivity σ (ms.m^{-1})
Coal	3	0.0001
Sandstone (wet)	20	0.1
Limestone	7	0.5

208

209 The simulation model is 250 m \times 100 m in size and symmetrical along the middle layer of
 210 the coal seam with a thickness of 10 m. The simulation grid step length is $\Delta x = \Delta y = 0.5\text{m}$, and the
 211 simulation time window $t_w = 30 \mu\text{s}$. A continuous sinusoidal wave with a frequency of 1 MHz and
 212 an amplitude of 10^5 is emitted in the coal seam. The initial position of the emission source was set
 213 at the position (50m, 50m), and 30 receivers were set within the position (55 m-200 m) with a
 214 spacing of 5 m. The schematic diagram of the numerical model is as follows:

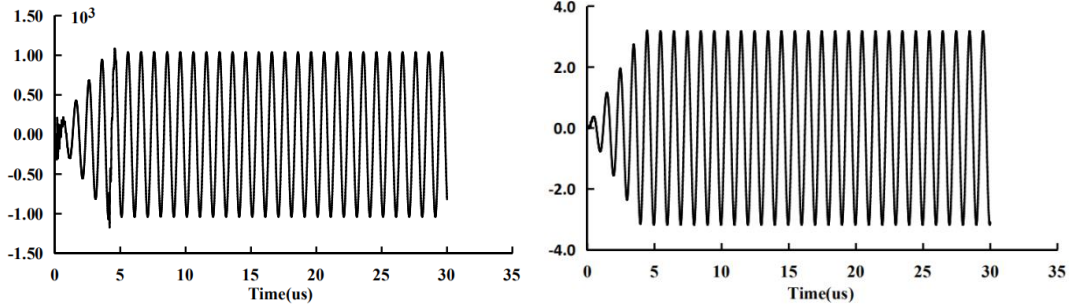


215

216 Fig.3 Numerical model for forward simulation of horizontal coal seam

217

218 Based on the above 2D model, the corresponding two-component numerical simulation
219 signals are obtained. Fig.4 shows the ez component of the electric field and hx component of the
220 magnetic field at the receiver at 70 m.



221

222 (a) ez component diagram of the electric field (b) hx component diagram of the magnetic field

223

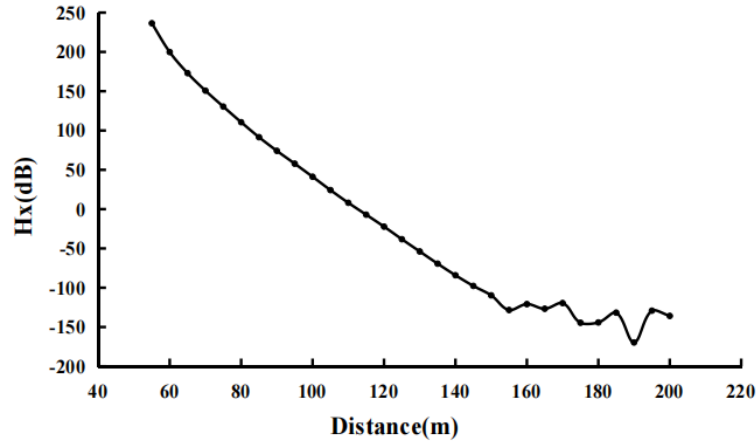
Fig.4 Signal diagram at 70 m of the horizontal model

224

225 The numerical simulation results generally show the characteristics of the sine wave. At the
226 first cycle of the sine wave, the waveform's amplitude is modulated, which has a slight influence
227 on the simulation results. Further, the hx component signals of each receiver in the same time
228 period are transformed by fast Fourier transform. The amplitude A corresponding to the frequency
229 of 1MHz in the transform result was selected to calculate the dB value of each received signal
230 according to Eq.(8):

231

$$dB = 20 \times \log A(f) \quad (8)$$



232

233

Fig.5 Energy attenuation curve of hx component of the radio wave

234

235

236

237

238

239

240

241

242

243

244

It can be seen from the curve of dB value with distance changing (Fig.5) that with the propagation of electromagnetic waves, the dB value of the hx component signal shows a regular attenuation trend before 150 m, which proves that the energy attenuation of radio waves propagating in the coal seam within the distance between the source and the receiver of 5 m-100 m is in line with the approximate linear attenuation law: the fitting attenuation coefficient of the hx component is about 5.4 dB/m. After 150 m, the energy is too small. Thus, the calculation error leads to a decrease in the data signal-to-noise ratio. But in general, dB attenuation of the hx component signal of the radio wave in the coal seam shows an approximately linear relationship with the propagation distance. This law lays the theoretical foundation for radio wave penetration tomography.

245

3.3 Forward simulation analysis of the inclined coal seam

246

247

248

249

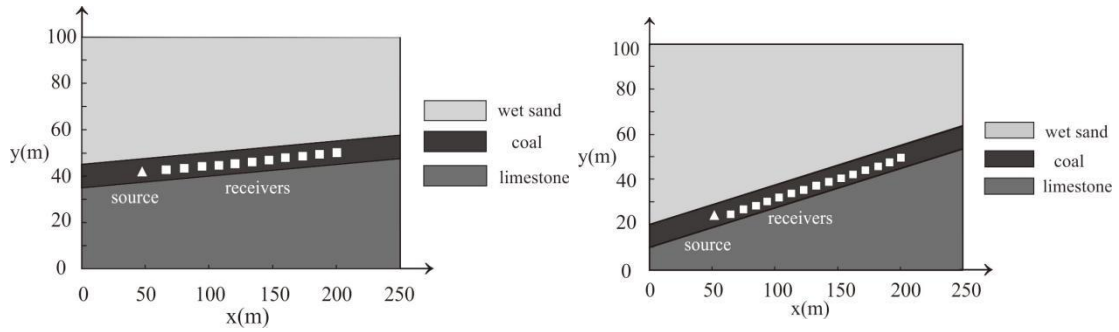
250

251

252

Several 2D models were constructed using the same medium material for the horizontal coal seam model to simulate the inclined coal seams of different inclinations. These models were 250 m × 100 m in size and had a coal seam thickness of 10 m (Table 1). During the experiment, the grid step length is set at $\Delta x = \Delta y = 0.5$ m, time window $t_w = 30$ μs , and the inclination as 1.1°, 3.4°, 5.6°, 7.8°, 10°, 11.1°, 12.2°, 14.3°, and 16.4°, respectively. Fig.6 shows two numerical simulation models of coal seam with an inclination of 3.4° and 11.1°, in which the electromagnetic wave was emitted at 50 m and the distance between receivers was set at 5 m (55 m - 200 m).

253



254

a) The model with an inclination of 3.4°

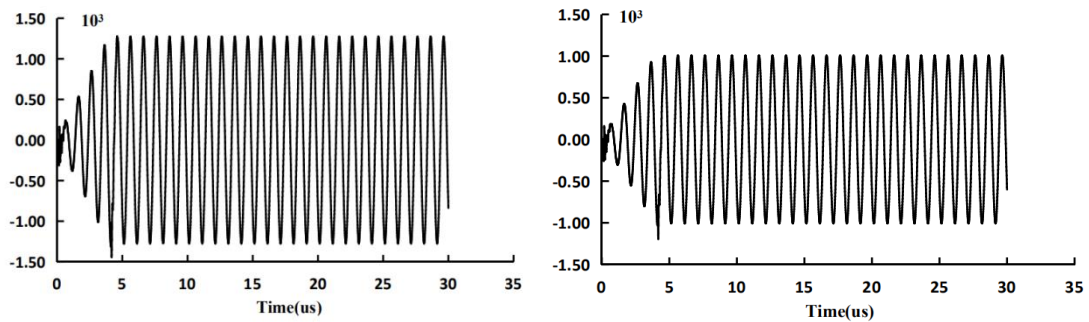
(b) The model with an inclination of 11.1°

255

Fig.6 2D numerical simulation model of coal seams with different inclinations

256

257



258

a) The electric field component (e_z) in the coal seam with an inclination of 3.4°

259

b) The electric field component (e_z) in the coal seam with an inclination of 11.1°

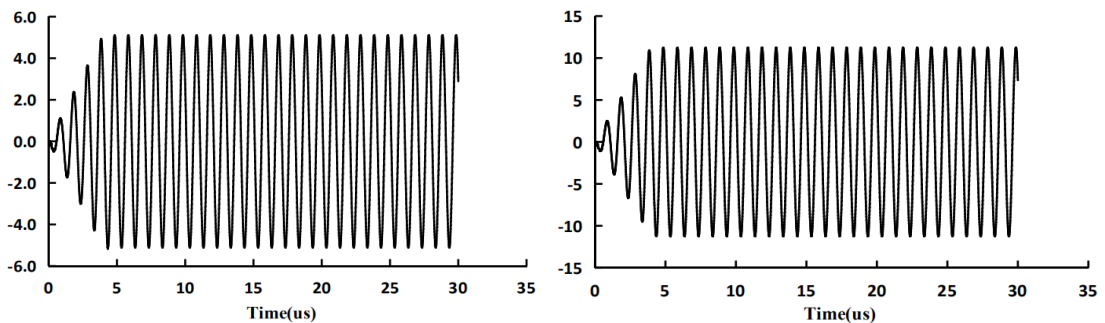
260

261

Fig.7 Electric field in coal seams with different inclination at 70 m

262

263



264

a) The magnetic field component (h_x) in the coal seam with an inclination of 3.4°

265

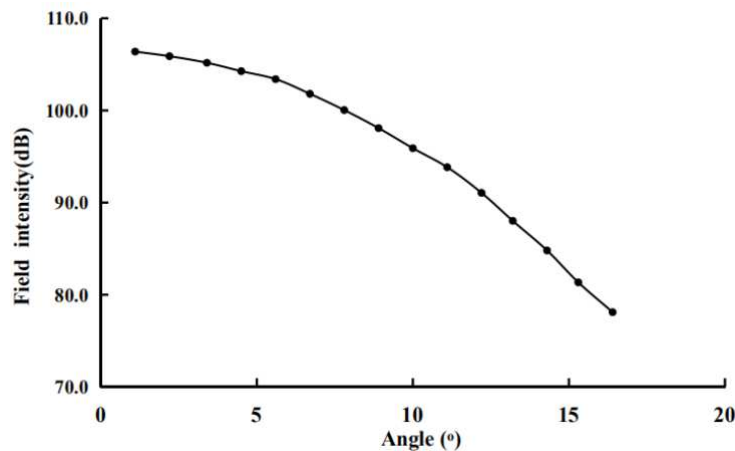
b) The magnetic field component (h_x) in the coal seam with an inclination of 11.1°

266 Fig.8 Magnetic field component in coal seams with different inclination at 70 m

267 Based on the 2D numerical model of the inclined coal seam (Fig.6), the numerically simulated
268 electric field e_z distribution (Fig.7), as well as magnetic field h_x distribution (Fig.8) of the inclined
269 coal seams can be obtained. Compared with the electric field component of the horizontal coal
270 seam in Fig.4(a), the inclination of the coal seam causes the reduction of the electric field
271 component. As the inclination of the coal seam increases, the electric field component decreases,
272 while the magnetic field component continuously increases. Therefore, it is more suitable to use
273 radio wave magnetic component data for inversion in the exploration of coal seams with great
274 inclination.

275 Compared with the magnetic field component diagram of the horizontal coal seam in Fig.4(b),
276 the inclination of the coal seam also affects the amplitude of the h_x component. To facilitate the
277 comparison with the 3D numerical simulation results, we selected the h_x component signal at 100
278 m in the numerical simulation result to calculate the dB value of the h_x component of coal seams
279 with different inclinations and analyzed the influence of changes in the inclination on the h_x
280 component. It can be seen from Fig.9 that at a position of 50 m from the horizontal source, as the
281 inclination of the coal seam increases, the dB value of the h_x component gradually decreases.

282



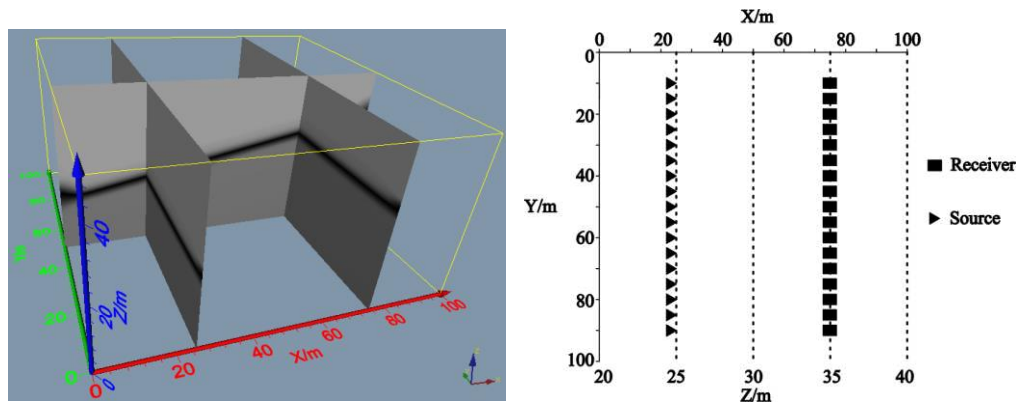
283

284 Fig.9 Energy attenuation of h_x component at 100 m with different inclinations

285

286 3.4 3D numerical simulation experiment

287 The parameters of the 3D simulation model are determined based on the 2D numerical
 288 simulation results with comprehensive consideration of other factors such as the effective
 289 propagation distance of radio waves, the influence of the inclination, and the coal seam thickness.
 290 The size of the 3D electrical model is 100m×100m×50m, and the coal seam is inclined 11.1° and
 291 10 m thick. Table 1 lists the parameters of the surrounding rock and coal seam. The mesh size is
 292 1m×1m×1m. The radio wave sources and receivers are set on the two lines with positions of x=25m
 293 and z=25m as well as x=75m and z=35m, respectively. The source spacing and the receiver spacing
 294 are both 5m. Thus, there are a total of 17 sources and 17 receivers. Fig.10 shows the 3D numerical
 295 simulation model of the inclined coal seam and the observation system. Consistent with the 2D
 296 simulation, a continuous sinusoidal wave with a frequency of 1 MHz and an amplitude of 10^5 is
 297 emitted in the coal seam. The simulation time window t_w is 30 μ s. We performed Fourier transform
 298 on the h_y component signal of each receiving point and selected the amplitude A corresponding to
 299 the frequency of 1MHz in the transform result to calculate the dB value of h_y at each received
 300 signal according to Eq.(8). The component dB value is used for imaging calculation after azimuth
 301 correction. Based on the conventional 2D attenuation imaging method and the method described
 302 in Section 2.2, the conventional 2D attenuation imaging results and the imaging results with coal
 303 seam undulation correction are obtained, respectively (Fig.11).



304

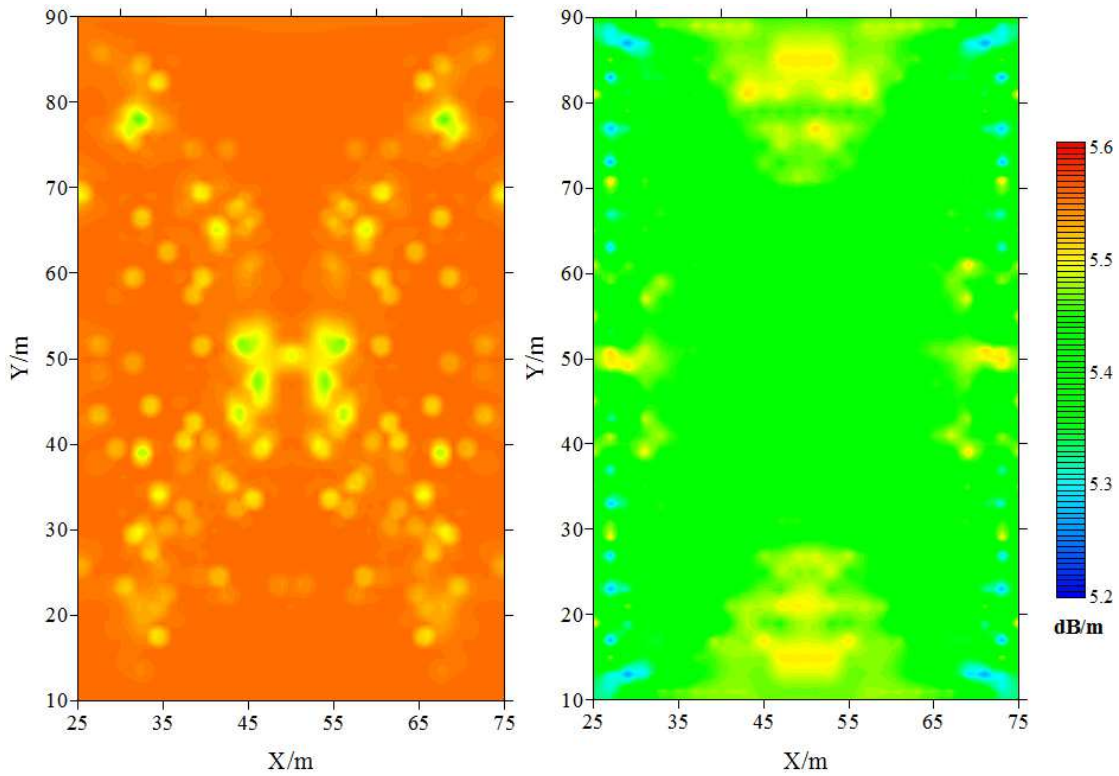
305

306 a) 3D model of a coal seam with an inclination of 11.1°

307 b) Observation system of 3D radio transmission simulation model

308

Fig.10 3D numerical simulation model and observation system



309

310 a) Results of conventional 2D electromagnetic wave attenuation coefficient imaging

311

312 b) Results of the improved electromagnetic wave attenuation coefficient imaging

313

314 Fig.11 Comparison of hy component numerical simulation imaging using different tomographic
315 methods

316

317 Fig.11a shows the results of the conventional 2D electromagnetic wave energy inversion
318 using 3D inclined coal seam numerical simulation data. The inversion results show that the energy
319 attenuation coefficient of the model is mainly concentrated at 5.55 dB/m, which is higher than 5.4
320 dB/m of the horizontal coal seam. In the 2D imaging calculation, the distance between the source
321 and receiver is a horizontal distance, which ignores the influence of the elevation on the
322 propagation distance. The existence of the elevation difference enlarges the actual propagation
323 distance between the source and receiver, so the inversion coefficient is larger than the actual
324 attenuation coefficient. When the elevation difference is constant, the smaller the distance between
325 the source and the receiver is, the greater the impact on the inversion results. The closer the

326 horizontal distance between the source and the receiver is, the greater the calculated attenuation
327 coefficient and the more the deviation from the real value.

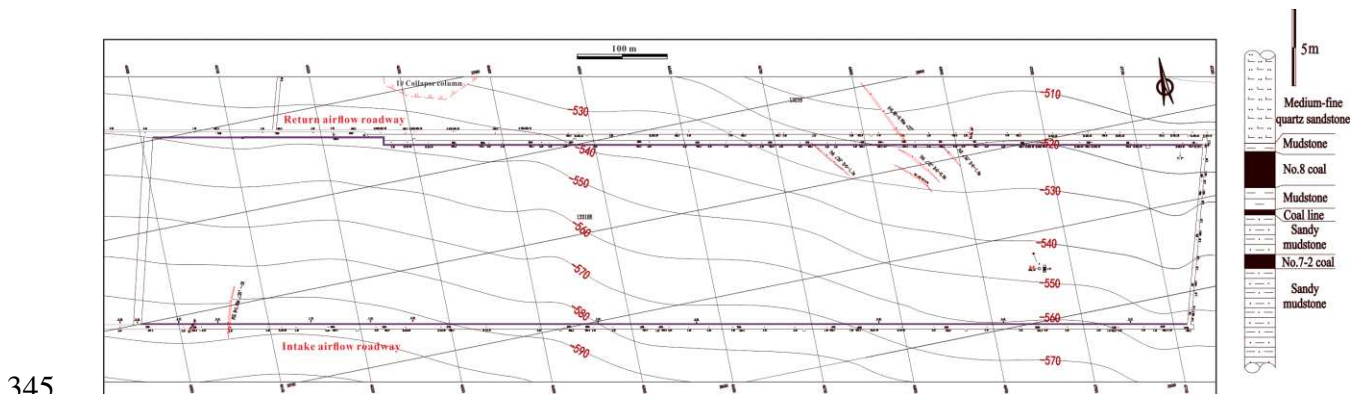
328 Fig.11b shows the electromagnetic attenuation imaging result after elevation correction.
329 Because this inversion method takes elevation into consideration, the inversion result is closer to
330 the real value, which indicates that the approximate 3D tomographic inversion method basically
331 eliminates the influence of the coal seam inclination on the tomographic inversion of
332 electromagnetic wave attenuation coefficient. Numerical simulation experiments further verify the
333 feasibility and effectiveness of the inversion method described in this study.

334

335 4. Field Test

336 4.1 Experiment site overview

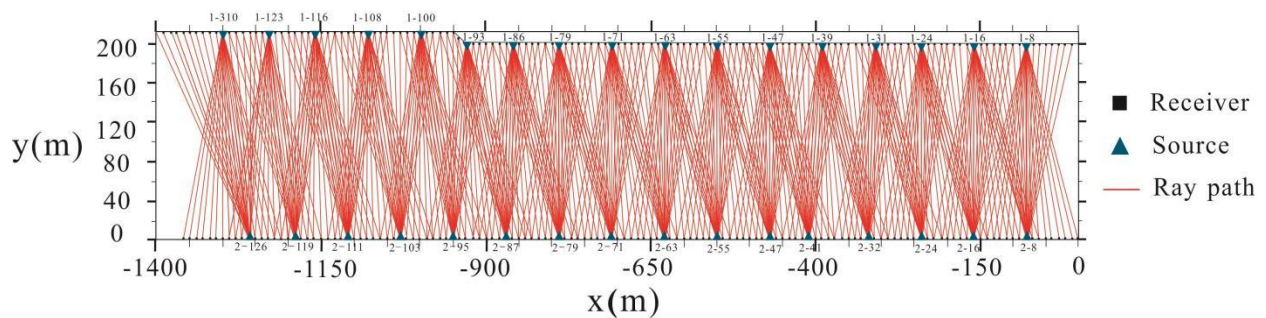
337 A coal mining face in Xieqiao mining area, Anhui Province, China, was selected as the
338 experimental site. The coal seam mined at this working face is No. 8 coal seam with the thickness
339 stabilized at 2.5 m and thinner local coal thickness due to structural influence. The overall shape
340 of the working face is a monoclinic structure with the coal (rock) layer inclination angle being 15°
341 on average, the elevation difference between the two detection roadways stabilized at about 50 m,
342 and a simple geological structure. In the actual measurement experiment, the transmission radio
343 wave energy attenuation coefficient in the coal seam is relatively small, which is more suitable for
344 the verification of the imaging method described in this study.



346 Figure 12 Contour map and comprehensive columnar shape of the measured coal seam working
347 face floor

348 4.2 Detection method and construction layout

349 In the experiment, WKT-6 radio wave tunnel perspective instrument was used, and the
350 transmitting source and receiving antenna with a frequency of 0.365 MHz were selected for
351 detection. The detection method adopts the fixed-point intersection method. A total of 33 emission
352 points were arranged every 80 m in the air inlet and return lanes. On the other side of the roadway,
353 receiving points were arranged every 10m, corresponding to each emission point. In addition, in
354 the fan-shaped symmetrical section of another roadway, 21 receiving points were set up to ensure
355 that each physical measurement point in the roadway was covered more than twice.



356

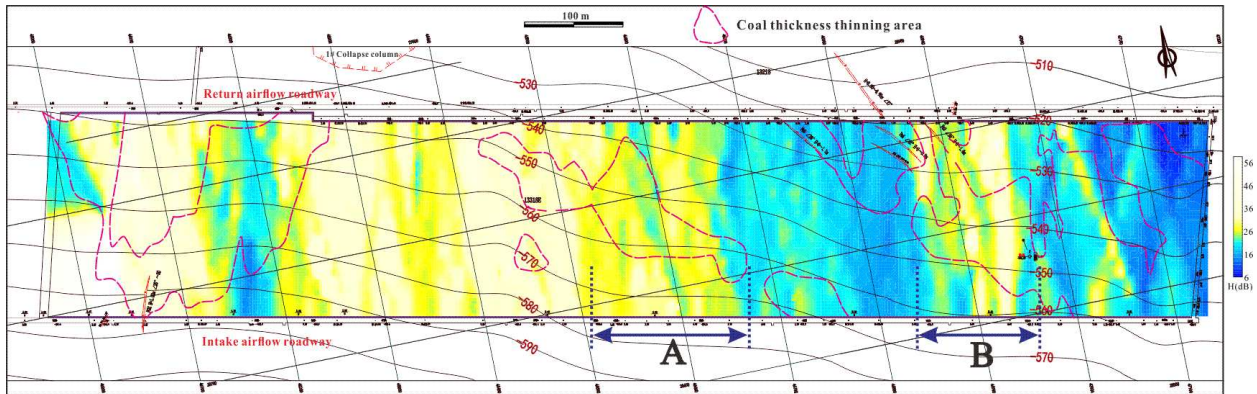
357 Figure 13 Observation system and ray path of the actual experiment

358 4.3 Test result comparison and analysis

359 According to the results of the measured transmitted radio wave field strength, the parameter
360 distribution in the coal seam working face was obtained by inversion. The higher the parameter is,
361 the more stable the coal seam; the lower the parameter is, the greater the possibility of abnormality.
362 The area delineated by the magenta dashed circle is the area where the coal thickness became
363 thinner after mining the work face. The blue area in Figure 14a generally corresponds well to the
364 coal thickness thinning area, indicating that radio wave exploration is highly sensitive to abnormal
365 coal thickness. But at the same time, there are two areas that do not correspond well, namely A
366 and B. The coal thicknesses in both A and B sections have become thinner, but the inversion
367 parameter values appear to be high values, which are inconsistent with the actual situation. Figure
368 14b shows the inversion result after terrain correction. The parameter values in the figure are
369 slightly reduced as a whole. In areas A and B, the inversion value decreases significantly and
370 coincides with the area where the coal thickness becomes thinner. The actual measurement
371 experiments show that the terrain correction method has achieved good application effects.

372

373

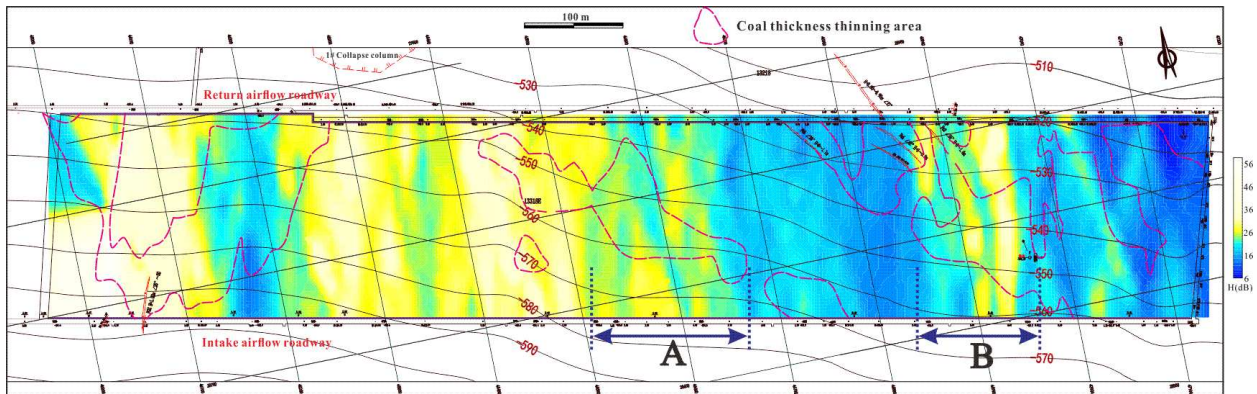


374

(a) Inversion results of the measured field strength values using the conventional two-dimensional method

375

376



377

(b) Inversion result of the measured field strength values using the improved method

378

Figure 14 Comparison of the inversion results of the measured field strength using two different methods

379

380

381

5. Conclusion

382

383

384

385

386

1) The dB value of radio electromagnetic waves in the coal seam attenuates in an approximately linear manner, and the linear tomographic inversion is suitable for electromagnetic wave attenuation imaging. The inclination of the coal seam has a great influence on the energy attenuation of radio waves. As the inclination increases, the electric field component decreases gradually, and the magnetic field component increases gradually.

387 2) This study proposes to use an approximate 3D inversion method to eliminate calculation
388 errors caused by coal seam undulation. 3D numerical simulation experiments and field test verified
389 the feasibility and effectiveness of the inversion method to eliminate the error caused by the
390 influence of the coal seam inclination on the tomographic inversion of electromagnetic wave
391 attenuation coefficient.

392

393 **Acknowledgments**

394 This work was supported by the Natural Science Study of the Department of Education, Anhui
395 Province (No. KJ2019A0125), Anhui Provincial Natural Science Foundation (No.
396 2008085QD185), and the Graduate innovation fund program of Anhui University of Science and
397 Technology (2020CX2002). Special thanks are given to the anonymous reviewers for their
398 assistance, comments, and suggestions.

399

400 **References**

401 Cheng J Y, Zhu M B, Wang Y H, et al. 2019. Cascade construction of geological model of longwall
402 panel for intelligent precision coal mining and its key technology [J]. Journal of China Coal
403 Society, 44(8): 2285-2295.

404

405 Giannopoulos A. 1997. The investigation of transmission-line matrix and finite-difference time -
406 domain methods for the forward problem of ground probing radar [D], University of York,
407 Department of Electronics, York, UK.

408

409 Han G H, Qu G R, Liu Z, et al. 2018. The Weighting Algorithms for the Landweber Method in
410 Electromagnetic Tomography [C]. Advances in Social Science, Education and Humanities
411 Research, 266.

412

413 Hu Z A, Zhang P S, Xu G Q. 2017. Research advances of seismic tomography technology in coal
414 seam [J]. Progress in Geophysics (In Chinese), 32(6): 2451-2459.

415

416 Hu Z A. 2019. Study on transmission seismic wave field and its 3D imaging technology in coal
417 mining face [D]. Anhui University of Science and Technology.
418

419 Hussain N, Karsiti M, Iqbal A. 2011. Forward modeling to study topography effects on EM signal
420 using FEM. IEEE.
421

422 Jackson M J, Friedel M J, Tweeton D R, et al. 1995. Three-dimensional imaging of underground
423 mine structures using seismic tomography [J]. Digital Library Home, 221-230.
424

425 Jol, H. M. 2011. Theory and Application of GPR[M]. Beijing: Electronic Industry Press.
426

427 L. G. Stolarczyk, S. S. Peng and Y. Luo. 2003. Imaging ahead of mining with radio imaging
428 method (RIM-IV) instrumentation and three-dimensional tomography [J]. Software Proceedings
429 of 22nd International Conference on Ground Control in Mining, Morgantown, WV, 136-143.
430

431 Li Y. 2015. The application of electromagnetic waves CT technology in the exploration of karst
432 [J]. Fujian Architecture, (06): 94-96.
433

434 Liu L, Zhao Z, Fan T. 2017. Comparison of several tomography methods for wireless radio wave
435 perspective [J]. Chinese Journal of Engineering Geophysics, 14(03): 277-283.
436

437 Liu S X, Ni J F. 2020. Review for cross-hole electromagnetic method. Progress in Geophysics (In
438 Chinese), 35(1): 0153-0165.
439

440 Liu X M, Liu S C, Jiang Z H, et al. 2013. Study on the tomography of radio-wave penetration
441 based on improved amplitude attenuation constant[J]. Progress in Geophys. (In Chinese), 28(2):
442 0980-0987.
443

444 Liu X L, Liu Z. 2019. A novel algorithm based on L1-L norm for inverse problem of
445 electromagnetic tomography [J]. Flow Measurement and Instrumentation, 65:318-326.
446

447 Liu Z X, Liu S C, Wang D W. 2013. Phase tomography technology of tunnel radio wave
448 perspective [J]. The Chinese Journal of Nonferrous Metals, 23(9): 2371-2378.
449

450 Peng S P, Zhang B, Wang T. 2015. China's coal resources: octothorpe shaped distribution
451 characteristics and sustainable development strategies [J]. Engineering Sciences, 17 (09): 29-35.
452

453 Peter K. Fullagar, Dean W. Livelybrooks, Ping Zhang, et al. 2000. Radio tomography and borehole
454 radar delineation of the McConnell nickel sulfide deposit, Sudbury, Ontario, Canada. Geophysics,
455 65(6):1920-1930.
456

457 Xiao Y L, Wu R X, Yan J P, et al. 2017. Field strength propagation law of radio wave penetration
458 and effective perspective width for coal face [J]. Journal of China Coal Society, 42 (3): 712-718.
459

460 Xiao Y L. 2017. Study on the characteristics of transmission seismic wave field in coal mining
461 face and its three-dimensional imaging technology [D]. Anhui University of Science and
462 Technology.
463

464 Hatherly, Peter. 2013. Overview on the application of geophysics in coal mining [J]. International
465 Journal of Coal Geology, 114:74-84
466

467 Yee K.S. 1966. Numerical solution of initial boundary value problems involving Maxwell
468 equations in isotropic media [J]. Antennas Propagat, 14(3): 302-307.
469

470 Yu Y B, Yue J H, Deng S Q. 2011. Electromagnetic wave propagation characteristics in high
471 resistivity coal seam [J]. Chinese Journal of Engineering Geophysics, 8(4): 412-416.
472

473 Yuan L, Zhang P S. 2019. Development status and prospect of geological guarantee technology
474 for precise coal mining [J]. Journal of China Coal Society, 44(8): 2277-2284.
475

476 Zhao D, Ding E, Xue H. 2013. Radio wave propagation characteristics in coal mine workplace [J].
477 Sensors & Transducers, 160(12):418-422.
478

- 479 Zhang H, Pan D M, Liu P, et al. 2016. Simulation and analysis of the influence of initial field
480 intensity on the inversion results. Progress in Geophysics (In Chinese), 31(6): 2788-2795.
481
- 482 Zhang M Z, Shi X M. 2009. Review of electromagnetic tomography technique [J]. Chinese
483 Journal of Engineering Geophysics, 6(04): 418-425.
484
- 485 Zhang P S, Hu Z A, Wu R X, et al. 2017. Coal Face Geological Structure and Application of
486 Anomalous Body Transmitting CT Integrated Imaging [J]. Coal Geology of China, 29(09): 49-52.